Hindawi
Modelling and Simulation in Engineering
Volume 2022, Article ID 2533714, 13 pages
https://doi.org/10.1155/2022/2533714

Research Article

Double-Diffusive MHD Viscous Fluid Flow in a Porous Medium in the Presence of Cattaneo-Christov Theories

Bidemi Olumide Falodun,[1] **Adeola John Omowaye**,[2] **Funmilayo Helen Oyelami**,[3] **Homan Emadifar**,[4] **Ahmed A. Hamoud**,[5] **and S. M. Atif**[6]

[1]*Department of Computer Science/Mathematics, Novena University, Ogume, Delta State, Nigeria*
[2]*Department of Mathematical Science, Federal University of Technology Akure, Akure, Nigeria*
[3]*Department of Mathematical and Physical Sciences, Afe Babalola University, Ado Ekiti, Nigeria*
[4]*Department of Mathematics, Hamedan Branch, Islamic Azad University, Hamedan, Iran*
[5]*Department of Mathematics, Taiz University, Taiz 96704, Yemen*
[6]*Department of Mathematics, Roots College International, DHA 1, Islamabad, Pakistan*

Correspondence should be addressed to Homan Emadifar; homan_emadi@yahoo.com

Received 21 February 2022; Accepted 2 August 2022; Published 18 August 2022

Academic Editor: Dimitris Drikakis

The Cattaneo-Christov model will be used to examine the significance of heat generation, viscous dissipation, and thermal radiation on a double-diffusive MHD flow in this study. In this study, it was discovered that heat and mass transfer can be affected by nonlinear buoyancy significance. The flow direction was subjected to a uniform magnetic field. A set of partial differential equations governs the current design (PDEs). In order to simplify these equations, they are converted into ordinary differential equations (ODEs). In order to numerically solve the nonlinear ODEs, the spectral relaxation method (SRM) is utilized. In order to decouple and linearize the equation sets, the SRM employs the Gauss-Seidel relaxation method. Geothermal power generation and underground storage systems are just a few examples where this research could be put to use. When compared to previous findings, the current outcomes were discovered to be closely related. Owing to an increase in Lorentz force, the imposed magnetic field slows down fluid motion. Viscosity dissipation and heat generation all contribute to the formation of an ever-thicker thermal boundary layer. When the Cattaneo-Christov models are used, the thermal and concentration boundary layers get a lot thicker.

1. Introduction

The wide range of free convection flow that occurs naturally and in building practice has been extensively studied by a number of scientists. Unpredictable driving possibilities arise when thermal and mass transport occurs simultaneously between transitions. Temperature angles and arrangement gradients can both contribute to a shift in vitality. The Dufour or diffusion thermo effect describes the synthesis-induced change in vitality. The Soret or thermodiffusion effect can also lead to mass transitions as a result of temperature gradients. When it comes to heat transfer processes, thermodiffusion and diffusion thermoeffects are of secondary importance compared to those recommended by Fick's or Fourier's theories. There are exceptions to every rule. Many equipment, like the MHD current generator and the Hall accelerator, use magnetohydrodynamic flows to transfer heat and mass, and recent advances in this area have been impressive [1–3]. Magnetic field effects on the motion of electrically executing viscous fluid with mass transport are also useful for the study of the planetary atmosphere. On an infinite vertical permeable slab by a tough magnetic field, Kinyanjui et al. [4] demonstrated the concurrent transfer of heat plus mass in a transient-free convection motion with radiative retention. An experiment by Yih [5] looked at the effects of velocity on thermal and solute transfer properties of mixed convection around a penetrable upright plate implanted in a submerged permeable channel under the

bonded influence of heat and mass diffusion. Mixed convection was studied by Elbashbeshy [6] in a permeable channel with an upright plate implanted in it. Research by Oyelami and Dada [7] investigated the impact of viscous dissipation on thermal transport by natural convection. It was found that viscous dissipation and chemical reactions affect thermal and mass transport in the Eyring-Powell fluid model studied by Oyelami and Dada [8]. Heat transport effects on incompressible fluid unsteady MHD flow were studied by Falodun and Fadugba [9]. Using an accelerated penetrable surface as a model, Fagbade et al. [10] scrutinized the MHD motion of a viscoelastic fluid passing through it. Falodun and Omowaye [11] investigated the convective flow of doubly diffusive thermal and mass transport in a thermal-stratification porous channel. Idowu and Falodun [12] recently looked at the thermophysical properties of non-Newtonian fluids that flow past an upright plate with holes when the Soret-Dufour mechanism is at work.

Fabrication calls for a stretching of the moving plate in its own plane so that it can work precisely and thermally with the fluid it is in contact with. Materials can stretch and shrink in a variety of ways. It was Crane [13] who first thought about two-dimensional flows on a stretched surface. Stratification is a property shared by all fluids contained within walls that have been heated to varying degrees. When the thermal boundary layer discharges constantly inside the fluid, the effects of thermal stratification can be observed. There can be thermal stratification when a hot fluid is discharged over a cool region, which results in a lighter fluid being deposited on top of a thicker fluid of equal density. In recent years, researchers have studied the analysis of flows derived from a hot surface and thermally stratified. Chemical and hydrometallurgical processes, in particular, experience thermal stratification as a result of heat transfer. Effects on flow over stretchable surfaces have become increasingly important. Expulsion of polymer, for example, will involve the object biting into dust and then continuing at a temperature appropriate for cooling. In light of the effects of thermal stratification, researchers have completed relevant research [14–17] in this manner. Some researchers have studied the MHD effects of Cattaneo-Christov theories in various energy-related currents triggered by the sheet's expansion. There are numerous processes in which MHD flows are taken into account. Examples include flow meters and power generators that use MHD technology, energy retrieval, plasma studies, aerodynamics, and solar energy equipment. In terms of heat flow, MHD's physical effects are significant. A large number of scientists have focused their attention on Cattaneo and Christov's heat transfer theories because of this. An additional relaxation time term was added by Cattaneo to Fourier's heat conduction law to create the Cattaneo-Christov Fourier thermal conduction law. As a result of Cattaneo's generalization of the modified Fourier heat conduction law, he established a single equation for temperature. Many fluid flow tests were conducted following the development of the Cattaneo-Christov model. In the squeezed flow of nanofluids, Muhammad et al. [18] addressed the Cattaneo-Christov thermal and mass fluxes. It was found that Hashim and Khan [19] utilized the Cattaneo-Christov thermal flow model for a Carreau fluid motion past a moving plate. Williamson hybrid nanofluids based on engine oil were studied by Jamshed et al. [20] for their reactions to the Cattaneo-Christov heat flow. Many scientists have been interested in studying fluid flow by stretching or shrinking films because of the practical applications in many design projects, such as paper and glass production, driving out polymer films and wires, drawing plastic films, turning filaments, and developing gemstones. Sakiadis [21] and Crane [13] were pioneering researchers in this field. Falodun et al. [22] carried out the MHD thermal and mass transport of Casson fluid motion research. A liquid Walter's-B fluid was discussed by Idowu and Falodun [23]. A non-Newtonian nanofluid flowing through a slanting plate was researched by Idowu and Falodun [24]. It was found that thermophoresis and thermal radiation plays a significance function in the unsteady MHD thermal and mass transport convection motion past a movable plate, as studied in [25]. According to Ahmed et al. [26], Soret-Dufour was utilized to address MHD heat and mass flow mechanisms.

In the literature, researchers are interested in the roles of thermal radiation, viscous dissipation, and heat generation in heat transport. Thermal radiation, viscous dissipation, and heat generation have applications in geothermal energy production and underground storage systems. Advanced energy conversion systems that operate at high temperatures rely heavily on thermal radiation. Nuclear power plants, rockets, satellites, gas turbines, and spacecraft are a few examples of this type of technology. As studied by Falodun and Ayegbusi [27], thermal radiation, viscous dissipation, and heat generation all had a significance on the motion of an electrically executing nanofluid. Bhatti and Abdelsalam [28] conducted experiments to address the significances of magnetic fields and thermal radiation on the bioinspired peristaltic drive of hybrid nanofluid. Internal heat generation, viscous dissipation, and thermal radiation were all explored when examining the peristaltic dynamics of a hybrid bionanofluid with a moderate Reynolds number by Abo-Elkhair et al. [29]. Idowu and Falodun [30] investigated how a steady free convection flow affected thermal radiation and magnetic fields in a porous channel. It was detected that thermal radiation, viscous dissipation, and heat generation all have an impact on the dynamics of a Casson fluid. An elastic surface was addressed by Zhang et al. [31], who analyzed the significance of magnetic field, thermal radiation, and viscous dissipation on the transport of a hybrid nanofluid. Entropy generation with heat transfer was used to study the three-dimensional motion of a hybrid nanofluid by Upreti et al. [32]. On a bidirectional porous surface, Joshi et al. [33] addressed the mixed convective flow of a magnetic hybrid nanofluid. Idowu et al. [34] investigated the transport of a dissipative Casson fluid in the presence of heat generation and viscous dissipation. An electrically executing fluid was explored by Falodun et al. [35] for its nonlinear viscous dissipative effect on an unsteady flow. For carbon nanotube nanofluids, Upreti et al. [36] discussed the significance of modified Arrhenius and thermal radiation on MHD transport. The slip transport of a micropolar fluid through a

wedge with heat evolution and viscous dissipation was determined analytically by Singh et al. [37]. It was discovered by Upreti et al. [38] that thermophoresis, suction, and injection all affect the free convective MHD transport of an Ag-kerosene oil nanofluid. Ramana Reddy et al. [39] investigated oscillatory mixed convective transport with chemical reaction and thermal radiation. Thermal radiation and viscous dissipation in an electrically conducting fluid were examined by Ramana Reddy et al. [40]. Reddy and Krishna [41] looked at thermal radiation and MHD heat transfer at a surface that is being stretched.

Using Cattaneo-Christov theories, studies have been done on the generation of heat, thermal radiation, and chemical reactions in a double-diffuse MHD flow. These facts serve as a backdrop to our investigation, which aims to better understand how heat is generated and how thermal radiation affects the chemistry-reacting MHD double diffusion flow. In the flow geometries, a porous medium is used to create the vertical plate. Thermal engineering, geothermal energy recovery, and underground storage systems will benefit greatly from this research. Engineers and scientists alike will benefit greatly from this research owing to its wide range of potential applications. SRM, a novel numerical technique, was employed in this research. Decoupling the differential equations is done using this method. There is a table with calculations for important engineering quantities and graphs that show how key parameters affect velocity, temperature, and concentration.

2. Mathematical Modeling

A steady case of incompressible two-dimensional MHD viscous fluid flow through a half-infinite vertical sheet folded in a penetrable medium which is thermally stratified is presented. Simulations were carried out with thermal radiation and concentration buoyancy significant. Infinite vertical sheet is placed such that x-axis is in vertical direction and the y-axis normal to the sheet. Wall temperature and concentration are considered as T_w and C_w, while T_∞ and C_∞ are the ambient temperature and concentration, respectively. The temperature difference $(\text{i.e.}, T_w - T_\infty)$ and concentration difference $(\text{i.e.}, T_w - T_\infty)$ determine the distributions of heat and mass transfer within the boundary layer. Since the plate as depicted in Figure 1 is considered to be cool, hence, $T_w < T_\infty$ and $C_w < C_\infty$. The velocities $u = 0$ and $v = 0$ at the wall because this paper considered no slip condition. Hence, the adhesive forces are greater than the cohesive forces. The Cattaneo-Christov theories of mass and heat flux are considered important. The contribution of density fluctuation with temperature plus concentration is elucidated to take place in body force term, and the variations in both concentration and temperature produce the buoyant force. A constant magnetism is supplied to the porous stretched sheet in a normal direction. Furthermore, it is believed that the flow is undergoing a homogeneous chemical reaction of first order with heat radiation. The energy transport phenomenon viscous dissipation effect is incorporated, whereas ohmic heating effect is neglected. It is also assumed the concentration of foreign mass is low due to which effects of Soret and Dufour effects are negligible. Being within the constraints and under the usual Boussinesq's approximation, the governing equations of the modeled problem are as follows (seen Falodun and Omowaye [11] and Idowu et al. [34]):

$$\frac{\partial u}{\partial x} + \frac{\partial v}{\partial y} = 0, \tag{1}$$

$$u\frac{\partial u}{\partial x} + v\frac{\partial u}{\partial y} = \nu\frac{\partial^2 u}{\partial y^2} - \frac{\nu}{k'}u - \frac{b}{k^*}(u)^2 - \frac{\sigma}{\rho}\beta_0^2 u + g\beta_t\left[(T - T_\infty) + (T - T_\infty)^2\right] + g\beta_c\left[(C - C_\infty) + (C - C_\infty)^2\right], \tag{2}$$

$$u\frac{\partial T}{\partial x} + v\frac{\partial T}{\partial y} = \alpha\frac{\partial^2 T}{\partial y^2} + \frac{\mu}{\rho c_p}\left(\frac{\partial u}{\partial y}\right)^2 - \frac{1}{\rho c_p}\frac{\partial q_r}{\partial y} + \frac{Q_0}{\rho c_p}(T - T_\infty) + -h_1\left[u\frac{\partial u}{\partial x}\frac{\partial T}{\partial x} + v\frac{\partial v}{\partial y}\frac{\partial T}{\partial y} + u\frac{\partial v}{\partial x}\frac{\partial T}{\partial x} + v^2\frac{\partial^2 T}{\partial y^2} + v\frac{\partial u}{\partial y}\frac{\partial T}{\partial x} + 2uv\frac{\partial^2 T}{\partial y \partial x} + u^2\frac{\partial^2 T}{\partial y^2}\right], \tag{3}$$

$$u\frac{\partial C}{\partial x} + v\frac{\partial C}{\partial y} = D_m\frac{\partial^2 C}{\partial y^2} - K_1(C - C_\infty) - h_2\begin{bmatrix} u\dfrac{\partial u}{\partial x}\dfrac{\partial C}{\partial x} + v\dfrac{\partial v}{\partial y}\dfrac{\partial C}{\partial y} + u\dfrac{\partial v}{\partial x}\dfrac{\partial C}{\partial x} \\ +v^2\dfrac{\partial^2 C}{\partial y^2} + v\dfrac{\partial u}{\partial y}\dfrac{\partial C}{\partial x} \\ +2uv\dfrac{\partial^2 C}{\partial y \partial x} + u^2\dfrac{\partial^2 C}{\partial y^2} \end{bmatrix}, \tag{4}$$

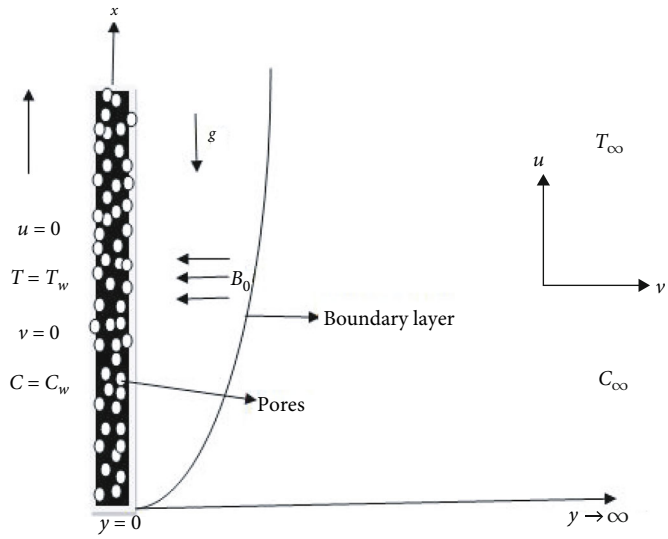

Figure 1: Physical configuration.

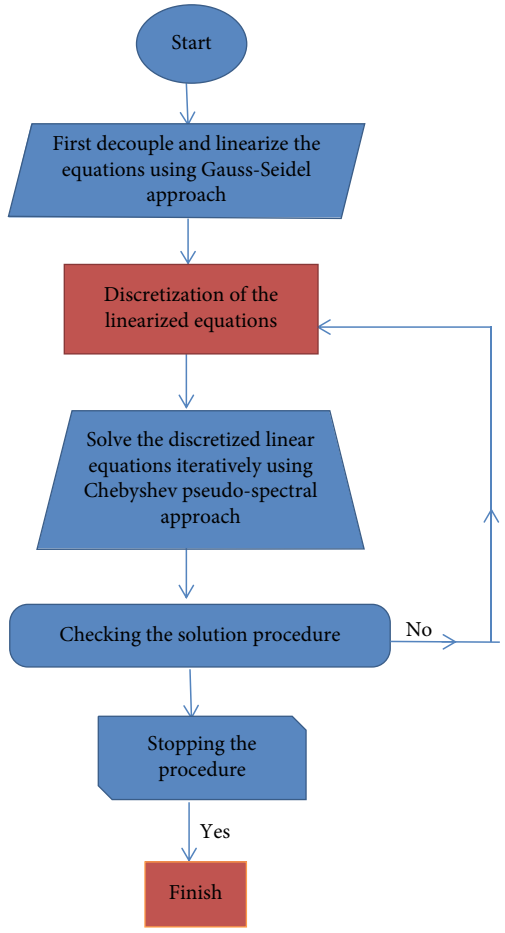

Figure 2: Flow diagram of the present solution technique.

with the corresponding boundary constraints

$$u = u_w(x) = ax, v = v_w(x), T = T_w, C = C_w, \quad \text{at } y = 0, \tag{5}$$

$$u \longrightarrow 0, T \longrightarrow T_\infty, C \longrightarrow C_\infty, \quad \text{as } y \longrightarrow \infty. \tag{6}$$

Here, $[u, v, 0]$ are the velocity elements along x and y directions. ν, σ, ρ, k', k^*, β_0, and g denote the viscosity, the electrical conductivity, the fluid density, the Darcy permeability, the Forchheimer parameter, the magnetic induction, and the acceleration owing to gravity, respectively. K_1 is the chemical reaction, c_p is the specific heat, and D_m is the mass diffusivity. β_t and β_c are the thermal and concentration expansion coefficients. The boundary constraints defined in Equations (5) and (6) are used to describe the flow behavior of the fluid within a solid boundary.

The wall temperature and concentration (T_w, C_w) with ambient temperature and concentration (T_∞, C_∞) are explained as follows (see Falodun and Omowaye [11]):

$$T_w - T_0 = m_1 x, T_\infty - T_0 = m_2 x, C_w - C_0 = m_3 x, C_\infty - C_0 = m_4 x. \tag{7}$$

The stream function $\Psi(x, y)$ is calculated as follows:

$$\Psi(x, y) = x\sqrt{a\nu} f(\eta). \tag{8}$$

The continuity equation is automatically satisfied. The similarity variables are given as follows (see Falodun and Omowaye [11]):

$$\eta = y\sqrt{\frac{a}{\nu}}, \theta(T_w - T_0) = T - T_0, \phi(C_w - C_0) = C - C_0, \tag{9}$$

substituting Equations (8) and (9) into Equations (2)–(4), and in boundary conditions (Equations (5) and (6)), we have

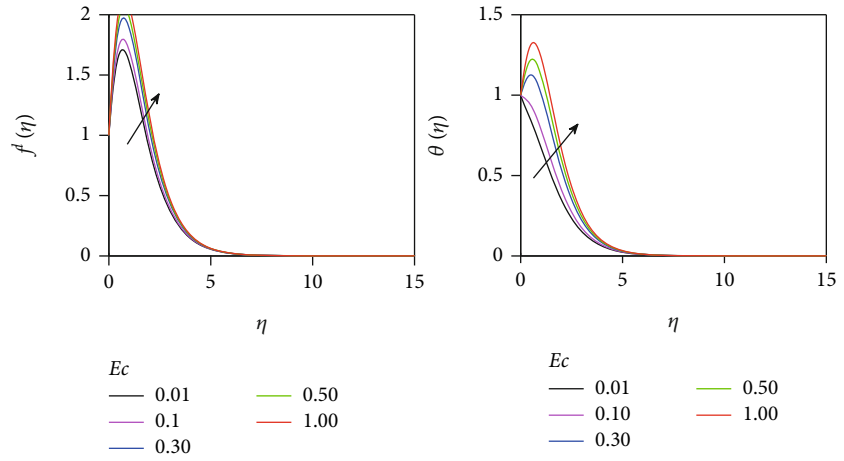

Figure 3: Significance of the viscous dissipation on velocity and temperature plots.

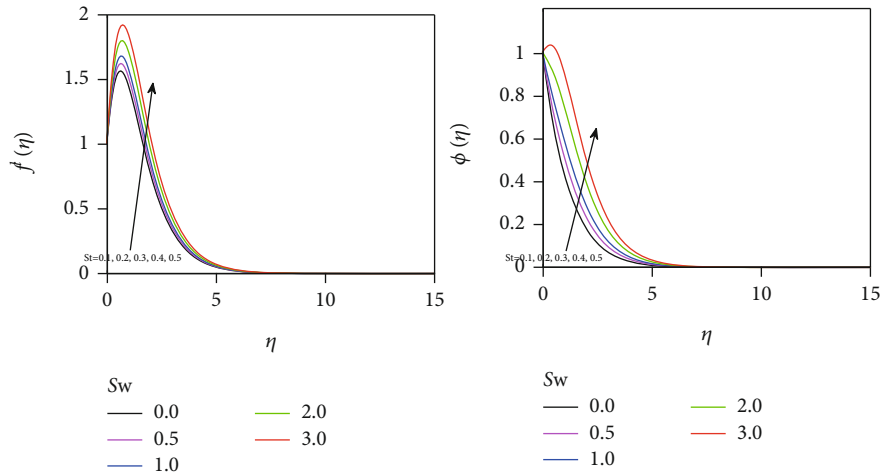

Figure 4: Significance of the suction and thermal stratification on velocity and concentration plot.

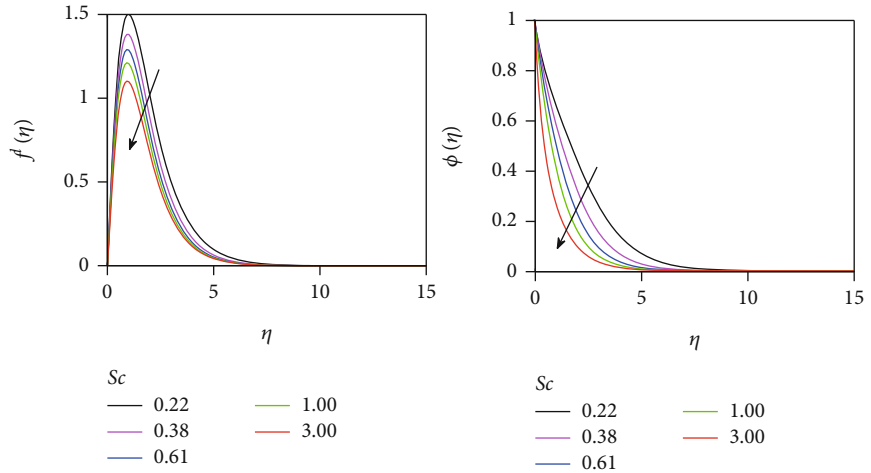

Figure 5: Significance of the Schmidt number on velocity and concentration plot.

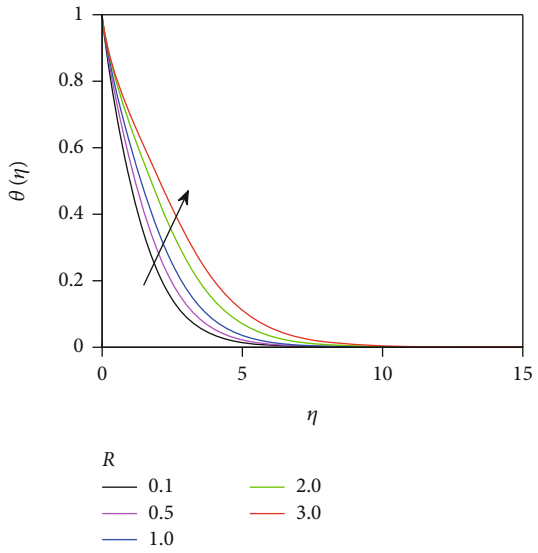

Figure 6: Significance of the radiation parameter on temperature plot.

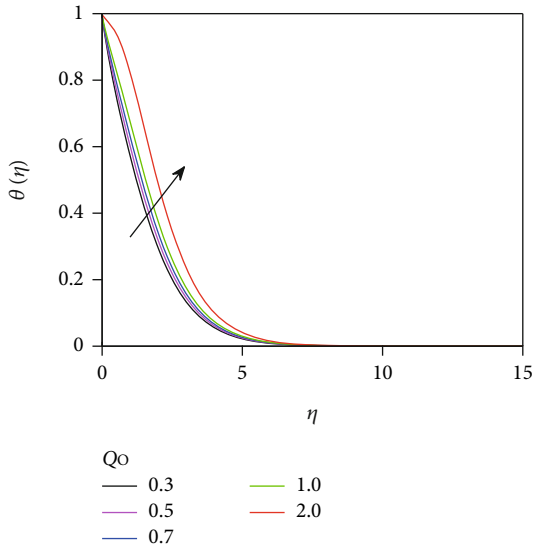

Figure 7: Significance of the heat generation on temperature plot.

the following:

$$f''' - (k_0 + M)f' - (\alpha^* + 1)f'^2 + ff'' + Gr\theta + \lambda_r\theta^2 + \lambda_m\phi^2 + \mathrm{Gm}\phi = 0, \tag{10}$$

$$(1+R)\theta'' + \mathrm{Pr}f\theta' + \mathrm{Pr}f'\theta + \mathrm{Pr}Ecf'^2 + Qo\theta - \beta_1\left(ff'\theta' + f^2\theta''\right) = 0, \tag{11}$$

$$\phi'' + \mathrm{Sc}f\phi' + \mathrm{Sc}f'\phi - \mathrm{ScRc}\phi - \beta_2\left(ff'\phi' + f^2\phi''\right) = 0. \tag{12}$$

The boundary constraints are presented as follows:

$$f'(\eta) = 1, f(\eta) = S_w, \theta(\eta) = (1 - \mathrm{St}), \phi(\eta) = (1 - \mathrm{St}), \quad \text{at}\,\eta = 0, \tag{13}$$

$$f'(\eta) \longrightarrow 0, \theta(\eta) \longrightarrow 0, \phi(\eta) \longrightarrow 0, \quad \text{as}\,\eta \longrightarrow \infty, \tag{14}$$

where $\mathrm{Gm} = (g\beta_c(C_w - C_0))/a^2x$ is the mass Grashof, $M = \sigma\beta_0^2/\rho a$ is the magnetic, $\mathrm{Gr} = (g\beta_t(T_w - T_0))/a^2x$ is the thermal Grashof number, $\lambda_r = (g\beta_t(T_w - T_0)^2)/a^2x$ is the nonlinear temperature buoyancy parameter, $\mathrm{Pr} = \nu/\alpha$ is the Prandtl number, $\lambda_m = (g\beta_c(C_w - C_0)^2)/a^2x$ is the nonlinear concentration buoyancy parameter, $\beta_1 = bh_1$ is the heat flux relaxation parameter, $\beta_2 = bh_2$ is the mass flux relaxation parameter, $\mathrm{Sc} = \nu/D_m$ is Schmidt, $k_0 = \nu/k'a$ is the permeability term, $\alpha^* = bx/k^*$ is the Forchheimer parameter, and $\mathrm{Rc} = K_1/a$ is the chemical reaction term.

The foremost important quantities for engineering are the skin friction and the Nusselt and Sherwood numbers. The local skin friction is given by $C_f = 2\tau_w/\rho U_0^2x^2$, where $\tau_w = \mu(\partial u/\partial y)|_{y=0}$ is the shear stress.

In dimensionless form, skin friction coefficient is $(\sqrt{x\,\mathrm{Re}}/2)C_f = f''(0)$.

The Nusselt number is defined as $\mathrm{Nu} = xq_w/k(T_w - T_0)$, where $q_w = -k(\partial T/\partial y)|_{y=0}$ is the heat flux. In dimensionless form, heat transfer rate is $\mathrm{Nu}/\sqrt{x\,\mathrm{Re}} = -\theta'(0)$.

The Sherwood number is defined as $\mathrm{Sh} = xJ_w/(D_m(C_w - C_0))$, where $J_w = -D_m(\partial C/\partial y)|_{y=0}$ is the mass flux. In dimensionless form, the mass transfer rate is $\mathrm{Sh}/\sqrt{x\,\mathrm{Re}} = -\phi'(0)$.

3. Method of Solution

To solve the Equations (10)–(12) subject to Equations (13) and (14), the SRM is utilized. SRM is an iterative method that uses the Gauss-Seidel approach in a systematic manner. Motsa [42] came up with this idea. If this method is used, the current iterations are evaluated at $(r+1)$, and linear and nonlinear terms are assumed to have been previously known at the previous iteration, denoted by (r). To use this method to solve systems of differential equations, you must first separate the system into its parts. Then, you must use the systematic Gauss-Siedel approach to write the system in a linear form. Use the implicit finite difference approach to solve the linear differential equations. The Chebyshev pseudospectral method is then used to solve the discretized linear differential equations. Figure 2 in this paper illustrates the algorithm showing the basic steps of SRM.

The approach has been utilized to solve diverse flow analysis by Falodun et al. [22], Motsa et al. [43], Alao et al. [44], and Idowu and Falodun [45].

Apply the SRM in Equations (10)–(12) considering Equations (13) and (14) to obtain the following:

$$f'''_{r+1} + a_{0,r}f'_{r+1} + a_{1,r} + a_{2,r}f''_{r+1} + a_{3,r} + a_{4,r} = 0, \tag{15}$$

$$b_{0,r}\theta''_{r+1} + b_{1,r}\theta'_{r+1} + b_{2,r}\theta_{r+1} + b_{3,r} + Qo\theta_{r+1} + b_{4,r}\theta'_{r+1} + b_{5,r}\theta''_{r+1} = 0, \tag{16}$$

$$\phi''_{r+1} + c_{0,r}\phi'_{r+1} + c_{1,r}\phi_{r+1} - \mathrm{ScRc}\phi_{r+1} + c_{2,r}\phi'_{r+1} + c_{3,r}\phi''_{r+1} = 0, \tag{17}$$

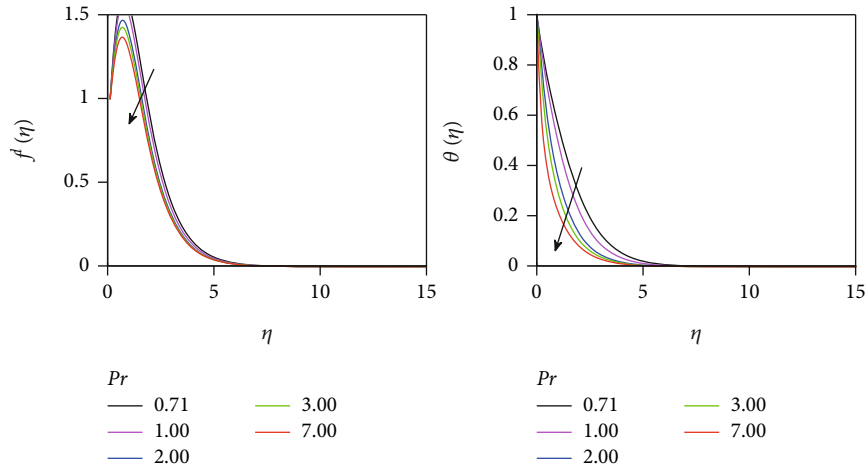

Figure 8: Significance of the Prandtl number on velocity and temperature plots.

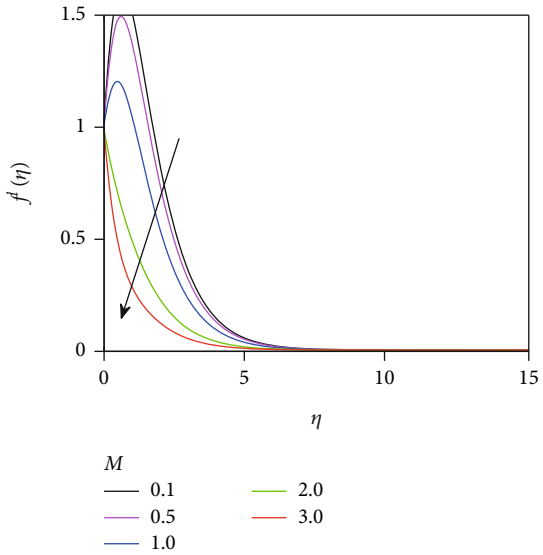

Figure 9: Significance of the magnetic parameter on velocity profile.

subject to

$$f_{r+1}(0) = 0, f'_{r+1}(0) = 1, \theta_{r+1}(0) = \phi_{r+1}(0) = 1, \tag{18}$$

$$f'_{r+1}(\infty) \longrightarrow 0, \theta_{r+1}(\infty) = \phi_{r+1}(\infty) \longrightarrow 0. \tag{19}$$

The parameter coefficients are defined as follows:

$$\begin{aligned} &a_{0,r} = -(k_0 + M), a_{1,r} = -(\alpha^* + 1) f'^2_r, a_{2,r} = f_r, a_{3,r} = \mathrm{Gr}\theta_r + \lambda_r \theta_r^2, \\ &a_{4,r} = \mathrm{Gm}\phi_r + \lambda_m \phi_r^2, b_{0,r} = (1 + R), b_{1,r} \mathrm{Pr} f_r, b_{2,r} = \mathrm{Pr} f'_{r+1}, b_{3,r} = \mathrm{Pr} E c f''^2_{r+1}, \\ &b_{4,r} = -\beta_1 f_{r+1} f'_{r+1}, b_{5,r} = -\beta_1 f^2_{r+1}, c_{0,r} = \mathrm{Sc} f_{r+1}, c_{1,r} = \mathrm{Sc} f'_{r+1}, \\ &c_{2,r} = -\beta_2 f'_{r+1} f_{r+1}, c_{3,r} = -\beta_2 f^2_{r+1}. \end{aligned} \tag{20}$$

An initial approximation is chosen to satisfy the boundary conditions in this study as follows:

$$f_0(\eta) = 1 - e^{-\eta}, f'_0(\eta) = e^{-\eta}, \theta_0(\eta) = \phi_0(\eta) = e^{-\eta}. \tag{21}$$

Starting from the above initial guess, Equations (15)–(17) are iteratively solved. Discretizing Equations (15)–(17) is by employing the Chebyshev collocation method, while implicit finite difference approach is utilized in the η-direction. The difference scheme is defined for the unknown functions as follows:

$$f\left(\eta_j\right) = \frac{f_j^{n+1} + f_j^n}{2}, \theta\left(\eta_j\right) = \frac{\theta_j^{n+1} + \theta_j^n}{2}, \phi\left(\eta_j\right) = \frac{\phi_j^{n+1} + \phi_j^n}{2}. \tag{22}$$

Applying the spectral approach on Equations (15)–(17) is to obtain the following:

$$\left[D^3 + a_{0,r} D + a_{2,r} D^2\right] f_{r+1} + a_{1,r} + a_{3,r} + a_{4,r} = 0, f'_{r+1}(\eta_0) = 1, f_{r+1}(\infty) = 0, \tag{23}$$

$$\left[b_{0,r} D^2 + b_{1,r} D + b_{2,r} + Q_0 + b_{4,r} D + b_{5,r} D^2\right] \theta_{r+1} + b_{3,r} = 0, \theta_{r+1}(\eta_0) = 1, \theta_{r+1}(\infty) = 0, \tag{24}$$

$$\left[D^2 + c_{0,r} D + c_{1,r} + c_{2,r} D - \mathrm{ScRc} + c_{3,r} D^2\right] \phi_{r+1} = 0, \phi_{r+1}(\eta_0) = 1, \phi_{r+1}(\infty) = 0. \tag{25}$$

We now apply the finite difference scheme on the equations above to obtain the following scheme:

$$A_1 f_j^{n+1} = B_1 f_j^n + K_1, \tag{26}$$

$$A_2 \theta_j^{n+1} = B_2 \theta_j^n + K_2, \tag{27}$$

$$A_3 \theta_j^{n+1} = B_3 \theta_j^n + K_3, \tag{28}$$

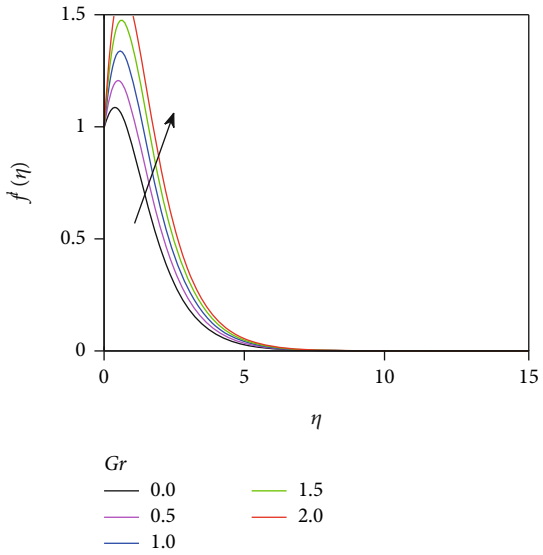

Figure 10: Significance of the thermal Grashof number on velocity plot.

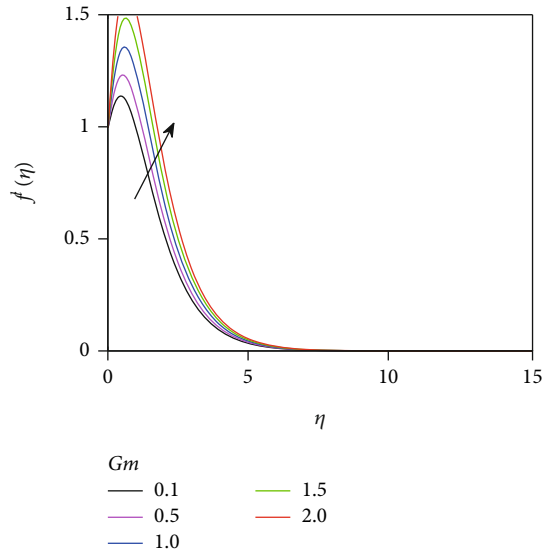

Figure 11: Significance of the mass Grashof number on velocity plot.

subject to the following constraints:

$$f'_{r+1}(\eta_0) = 1, \theta_{r+1}(\eta_0) = \phi_{r+1}(\eta_0) = 1,$$
$$f'_{r+1}(\eta_{Nx}) = 0, \theta_{r+1}(\eta_{Nx}) = \phi_{r+1}(\eta_{Nx}) = 0, \quad (29)$$

where

$$A_1 = \frac{D^3 + a_{0,r}D + a_{2,r}D^2}{2},$$
$$B_1 = -\frac{D^3 + a_{0,r}D + a_{2,r}D^2}{2},$$
$$K_1 = -a_{1,r}^{n+1} - a_{3,r}^{n+1} - a_{4,r}^{n+1},$$
$$A_2 = \frac{b_{0,r}D^2 + b_{1,r}D + b_{2,r} + Qo + b_{4,r}D + b_{5,r}D^2}{2},$$
$$B_2 = -\frac{b_{0,r}D^2 + b_{1,r}D + b_{2,r} + Qo + b_{4,r}D + b_{5,r}D^2}{2}, \quad (30)$$
$$K_2 = -b_{3,r}^{n+1},$$
$$A_3 = \frac{D^3 + c_{0,r}D + c_{1,r} + c_{2,r}D - \mathrm{ScRc} + c_{3,r}D^2}{2},$$
$$B_3 = -\frac{D^3 + c_{0,r}D + c_{1,r} + c_{2,r}D - \mathrm{ScRc} + c_{3,r}D^2}{2},$$
$$K_3 = 0.$$

4. Discussion of Results

Figures 3–15 depict the flow parameters' influence on the velocity, temperature, and concentration profiles. Figure 3 shows the significance of the Eckert number Ec on the temperature and velocity plots of the viscous dissipation parameter. The fluid's motion is accelerated by a high Eckert number, as shown in Figure 3. Ec is a measure of the flow's kinetic energy in relation to its enthalpy. When Ec rises,

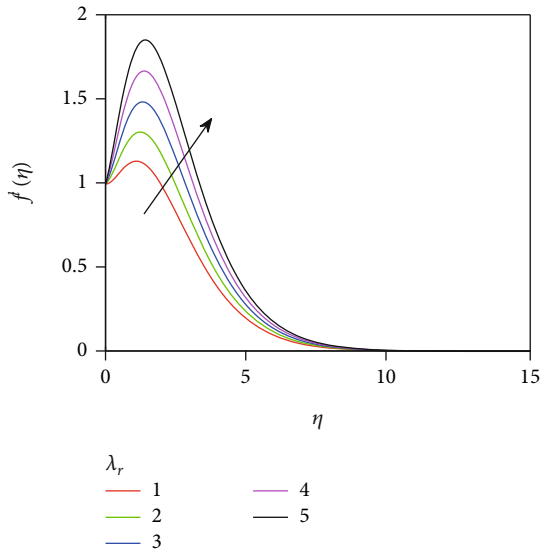

Figure 12: Significance of the nonlinear convective temperature parameter on velocity plot.

more heat energy is dissipated through viscous dissipation and entered into the energy equation. Increasing the velocity profile in Figure 3 is one way this heat energy aids fluid particle heating and acceleration. Accelerating and increasing buoyancy force are two of the benefits of using Ec. Both velocity and temperature increase as the Eckert number rises. In other words, in addition to the thermally stratified medium, a high value of Ec increases momentum and the thickness of the thermal boundary layer. The Eckert number, which is a physical representation of this relationship, relates effective transport and heat release potential. So, the difference in temperature between the wall and the free flow $(T_w - T_\infty)$ has a big effect on how hot or cold fluid particles are in the boundary layer.

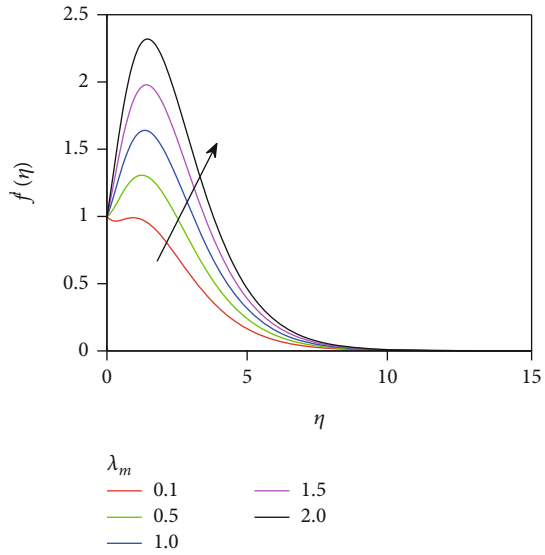

Figure 13: Significance of the nonlinear convective concentration parameter on velocity plots.

Thermal stratification and suction velocity are both shown in Figure 4 as potential influencers on velocity and concentration profiles. Both the velocity and concentration profiles improve when the thermal stratification values and the suction velocity are raised. By increasing the velocity of the fluid particles, positive suction velocity acts as a force on fluid flow. Solute boundary layer thickness and momentum increase as pressure is applied to the fluid flow in the thermally stratified porous medium. As a result, both suction velocity and flow rate are accelerated by thermal stratification. Consequently, the velocity and solute layers thicken significantly. When two fluids of varying temperatures come into contact, thermal stratification occurs. Physical properties like viscosity, density, and specific heat capacity increase to speed up the thickness of the boundary layer. In this study, heat generation and viscous dissipation cause the temperature in the thermal stratification region to rise.

Figure 5 depicts the influence of the Schmidt number Sc on the velocity and concentration profiles. The Schmidt number is critical in this study because it tells us how thick the viscous and concentration boundary layers are. The effect of the Schmidt number on concentration is similar to that of the Prandtl number on temperature. There is a decrease in the concentration profile when the Schmidt number is increased. The inverse of the Brownian diffusion coefficient is the Schmidt number. As a result, when the Schmidt momentum is increased, Brownian diffusion is weakened, and the concentration profile is immediately reduced. According to our numerical simulation, increases in the Schmidt number result in the same rate of species' spontaneous diffusion. Species diffusion exceeds momentum diffusivity when the Schmidt number is less than one. In other words, there is no species concentration if you set the Schmidt number to 0. A high Schmidt number indicates that momentum diffusion is more important than mass flux in the physical world. However, it is worth noting that the Schmidt number increases with dynamic viscosity, while density and mass diffusivity decrease the Schmidt number. Because of this, the Schmidt number is used to measure the amount of mass transfer in boundary layer flows.

When the thermal radiation parameter is increased, a temperature increase is shown in Figure 6. This is because the higher the radiation parameter, the more heat is transferred to the boundary layer region. The fluid in the thermal boundary layer is heated by using the Roseland approximation to approximate the radiant heat flux. Radiant heat plays a critical role in the transfer of heat at extremely high temperatures. However, increasing R improves the fluid's thermal condition.

When the heat generation parameter is increased or decreased, the temperature changes in Figure 7. The temperature rises as the heat generation parameter increases. The difference in temperature between the fluid and the free stream is the physical basis for the term "heat generation." An increase in the heat generation parameter, therefore, translates into a higher flow rate and a higher temperature for a given fluid. As a result, the free stream's temperature is minuscule. So, when the heat generation parameter and the thermally stratified medium have high values, you can expect the temperature profile and the thickness of the thermal boundary layer to rise.

Figure 8 depicts the impact of the Prandtl number on the velocity and temperature profile. The velocity profiles narrow as the Prandtl number rises. Temperature gradients near the surface are greater at higher Prandtl numbers, and the temperature drops significantly as a result. Figure 8 shows that the temperature decreases as the Prandtl number increases because of excessive stratification. That means thermal diffusivity controls flow, while momentum diffusivity controls flow behavior. Controlling the rate at which an electrically conductive fluid cools is therefore advantageous. In this experiment, the temperature of the wall and the temperature of the free stream, along with the thickness of the thermal boundary layer, cause the water to cool.

When a magnetic field parameter is present, it can be seen in Figure 9. The Lorentz force is generated as a result of the imposed magnetism. Due to the Lorentz force's slowing properties, it is expected that the flow will be suppressed. When the magnetic parameter has a large value, the Lorentz force is stronger. This makes the velocity profile and overall thickness of the boundary layer become even more similar.

Using the Grashof number, the velocity distribution is shown in Figure 10. As the buoyancy parameter goes up, the flow speeds up because the thermal buoyancy helps the flow of fluids in the boundary layer. It is shown in Figure 11 that the modified Grashof number has an effect on velocity. One can see an increase in the velocity profile with a rising modified Grashof number. Figures 12 and 13 depict the nonlinear convective parameters temperature (λ_r) and concentration (λ_m). λ_r can be seen to improve the velocity profile in Figures 12 and 13. Thermal and mass boundary layers are buoyant due to a nonlinear buoyancy force. As a result, increasing the nonlinear convective parameter increases the buoyancy force, which in turn increases the drag force by increasing velocity and the total hydrodynamic boundary layer thickness. The heat flux

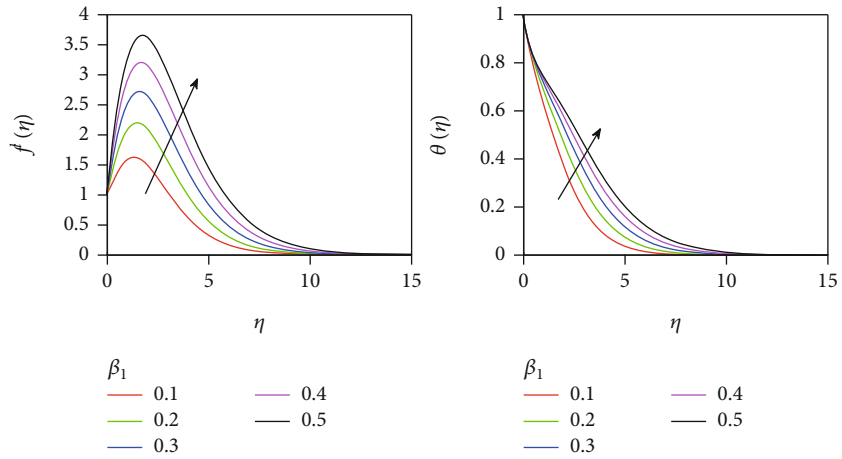

Figure 14: Significance of the thermal flux relaxation parameter on velocity and temperature plots.

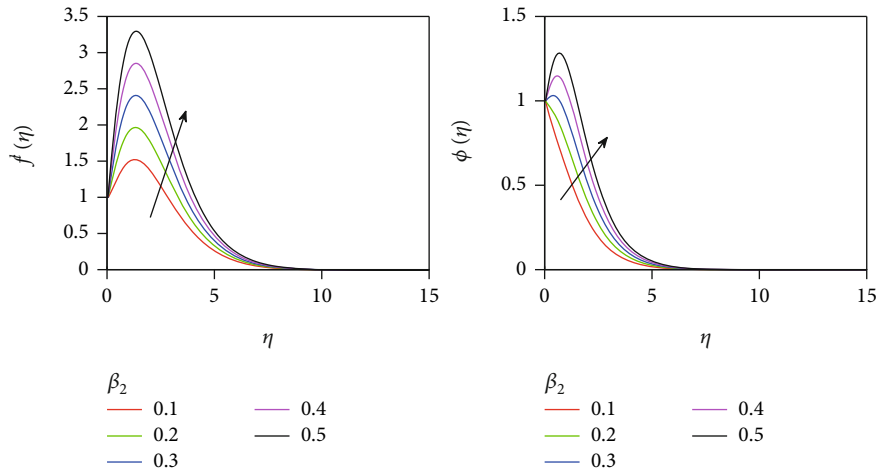

Figure 15: Significance of the mass flux relaxation parameter on velocity and concentration plots.

Table 1: Comparison of the present study solved using SRM and that of Besthapu et al. [14] solved using SHAM.

Gr	Besthapu et al. [14] (SHAM solution)			Present result (SRM solution) when $R = Q_0 = 0$		
	$-f''(0)$	$-\theta'(0)$	$\phi'(0)$	$-f''(0)$	$-\theta'(0)$	$\phi'(0)$
0.0	1.24193395	0.59113154	2.80938835	1.24193381	0.59113144	2.80938835
0.5	1.02710038	0.59947136	2.80110453	1.02710036	0.59947112	2.80110451
1.0	0.81565774	0.60736531	2.79307309	0.82565762	0.60736525	2.79307308
2.0	0.40184567	0.62177831	2.77768697	0.40184565	0.62177841	2.77768697

relaxation parameter (β_1) effect on velocity and temperature profiles is shown in Figure 14. The velocity and temperature distributions are improved by increasing β_1. When thermal radiation and heat generation are included in the energy equation, the temperature distribution of the boundary layer's fluid particles increases. As a result, the temperature and overall thickness of the thermal buoyancy layer rise when thermal radiation and heat generation increase. Using the mass flux relaxation parameter (β_2), the velocity and concentration profiles are shown in Figure 15. The velocities and concentration profiles were found to increase with an increase in β_2. Figures 14 and 15 show double-diffusive flow (heat and mass transfer) with both heat production and heat loss.

This study was solved using SRM, whereas Besthapu et al. [14] used SHAM. Table 1 shows the comparison. The results of this study are exactly the same as the results of

Table 2: Calculations of skin friction coefficient (C_f) and the Nusselt number (Nu) for different flow parameters.

k_0	M	Gr	R	Pr	Sc	St	C_f	Nh	Sh
0.1	1.00	2.0	0.4	0.71	3.0	0.01	1.4197	0.6360	0.6993
0.2	1.00	2.0	0.4	0.71	3.0	0.01	1.4176	0.6335	0.6993
0.3	1.00	2.0	0.4	0.71	3.0	0.01	1.4154	0.6309	0.6993
0.1	0.00	2.0	0.4	0.71	3.0	0.01	2.5456	0.6885	0.5112
0.1	0.50	2.0	0.4	0.71	3.0	0.01	1.2389	0.6885	0.5112
0.1	1.00	2.0	0.4	0.71	3.0	0.01	1.1558	0.6885	0.5112
0.1	1.00	1.0	0.4	0.71	3.0	0.01	0.6625	0.6102	0.5001
0.1	1.00	2.0	0.4	0.71	3.0	0.01	1.4217	0.6102	0.5001
0.1	1.00	3.0	0.4	0.71	3.0	0.01	2.1808	0.6102	0.5001
0.1	1.00	2.0	0.5	0.71	3.0	0.01	0.9635	0.5320	0.6993
0.1	1.00	2.0	1.0	0.71	3.0	0.01	1.0474	0.5349	0.6993
0.1	1.00	2.0	1.5	0.71	3.0	0.01	1.1572	0.5481	0.6993
0.1	1.00	2.0	0.4	0.71	3.0	0.01	1.7808	1.0390	1.3548
0.1	1.00	2.0	0.4	1.00	3.0	0.01	1.5475	0.7255	1.3548
0.1	1.00	2.0	0.4	7.00	3.0	0.01	1.4217	0.6385	1.3548
0.1	1.00	2.0	0.4	0.71	0.6	0.01	1.0610	0.6385	0.5650
0.1	1.00	2.0	0.4	0.71	1.0	0.01	1.2611	0.6385	0.6145
0.1	1.00	2.0	0.4	0.71	2.0	0.01	1.4273	0.6385	0.7033
0.1	1.00	2.0	0.4	0.71	3.0	0.01	1.4982	0.6497	0.7912
0.1	1.00	2.0	0.4	0.71	3.0	0.02	1.4545	0.6585	0.7384
0.1	1.00	2.0	0.4	0.71	3.0	0.03	1.3916	0.6585	0.6632

other studies. Calculated values of C_f, Nu, and Sh are shown in Table 2 for a variety of flow parameters, such as k_0 and a wide range of k, M, Gr, R, Sc, and St. The Sherwood and Nusselt numbers have no effect on the sheath friction coefficient when k_0 is large. The skin friction coefficient decreases with a large value of M, but the Sherwood and Nusselt numbers are unaffected. When Gr is increased, the skin friction coefficient also rises in proportion to it. A possible explanation for this is that the buoyancy force is causing the momentum boundary layer to thicken more rapidly. The sheath friction coefficient and the Nusselt number rise in direct proportion to the value of R. Thus, a high R value increases the rate of heat transfer, as can be seen here. The sheath friction coefficient and the Nusselt number both worsen when Pr increases, whereas when Sc rises, the sheath friction coefficient is worsened and the mass transport rate is increased via the Sherwood number. The skin friction coefficient decreases as the stratification parameter (St) is raised. As with Sherwood, the rate at which heat is transferred increases with an increase in St.

5. Conclusion

In this study, numerical simulations have been used to investigate the significances of thermal radiation, viscous dissipation, and heat generation on double-diffusive MHD convective heat and mass transport boundary layer flow past a stretchable sheet situated in a thermally stratified penetrable channel. The following are the study's major conclusions:

(i) Heat and mass are transported more quickly when the velocity and temperature are elevated due to the viscous dissipation effect

(ii) Raising the thermal stratification and suction parameter has a big effect on the velocity and concentration plots because it makes the distributions rise

(iii) As the thermal radiation goes up, the temperature plot goes up, which helps improve the thermal state of the fluid

(iv) The speed and thickness of the hydrodynamic boundary layer are both reduced by a magnetic field

Because of the presence of a magnetic field, these findings are expected to be useful in controlling the flow of turbulence in the boundary layer. Use of high polymer additives in petroleum pipelines can also benefit commercially from this technique. Thermal radiation is used a lot in the making of ceramics and glass, as well as in the development of high-temperature advanced energy conversion systems.

All aspects of viscous fluid heat and mass transfer, and the steady flow of electrically conductive and chemically reacting fluids are all aspects of this study. However, there are still a lot of possibilities for further investigation into this type of issue. For your convenience, the following are some of these instances:

(i) Newtonian hybrid nanofluids for turbulent flow regimes can be studied in this manner

(ii) Extending it to a wedge with the effects of joule and ohmic heating is possible

Data Availability

Data is available upon reasonable request falodunbidemi2014@gmail.com.

Conflicts of Interest

The authors declare that they have no conflicts of interest.

References

[1] F. H. Oyelami and B. O. Falodun, "Heat and mass transfer of hydrodynamic boundary layer flow along a flat plate with the influence of variable temperature and viscous dissipation," *International Journal of Heat and Technology*, vol. 39, no. 2, pp. 441–450, 2021.

[2] F. H. Oyelami, E. O. Ige, O. Y. Saka-Balogun, and O. A. Adeyemo, "Study of heat and mass transfer to magnetohydrodynamic (MHD) pulsatile couple stress fluid between two parallel porous plates," *Instrumentation Mesure Métrologie*, vol. 20, no. 4, pp. 179–185, 2021.

[3] F. H. Oyelami, E. O. Ige, N. O. Taiyese, and O. Y. Saka-Balogun, "Magneto-radiative analysis of thermal effect in symmetrical stenotic arterial blood flow," *Journal of Mathematical and Computational Science*, vol. 11, no. 5, pp. 5213–5230, 2021.

[4] M. Kinyanjui, J. K. Kwanza, and S. M. Uppal, "Magnetohydrodynamic free convection heat and mass transfer of a heat generating fluid past an impulsively started infinite vertical porous plate with Hall current and radiation absorption," *Energy Conversion and Management*, vol. 42, no. 8, pp. 917–931, 2001.

[5] K. A. Yih, "The effect of transpiration on coupled heat and mass transfer in mixed convection over a vertical plate embedded in a saturated porous medium," *International Communications in Heat and Mass Transfer*, vol. 24, no. 2, pp. 265–275, 1997.

[6] E. M. A. Elbashbeshy, "The mixed convection along a vertical plate embedded in non-Darcian porous medium with suction and injection," *Applied Mathematics and Computation*, vol. 136, no. 1, pp. 139–149, 2003.

[7] F. H. Oyelami and M. S. Dada, "Unsteady magnetohydrodynamic flow of some non-Newtonian fluids with slip through porous channel," *International Journal of Heat and Technology*, vol. 36, no. 2, pp. 709–713, 2018.

[8] F. H. Oyelami and M. S. Dada, "Numerical analysis of non-Newtonian fluid in a non-Darcy porous channel," *Modelling, Measurement and Control*, vol. 87, no. 2, pp. 83–91, 2018.

[9] B. O. Falodun and S. E. Fadugba, "Effects of heat transfer on unsteady magnetohydrodynamics (MHD) boundary layer flow of an incompressible fluid a moving vertical plate," *World Scientific News*, vol. 88, no. 2, pp. 118–137, 2017.

[10] A. I. Fagbade, B. O. Falodun, and A. J. Omowaye, "MHD natural convection flow of viscoelastic fluid over an accelerating permeable surface with thermal radiation and heat source or sink: spectral homotopy analysis approach," *Ain Shams Engineering Journal*, vol. 9, no. 4, pp. 1029–1041, 2018.

[11] B. O. Falodun and A. J. Omowaye, "Double-diffusive MHD convective flow of heat and mass transfer over a stretching sheet embedded in a thermally-stratified porous medium," *World Journal of Engineering*, vol. 16, no. 6, pp. 712–724, 2019.

[12] A. S. Idowu and B. O. Falodun, "Effects of thermophoresis, Soret-Dufour on heat and mass transfer flow of magnetohydrodynamics non-Newtonian nanofluid over an inclined plate," *Arab Journal of Basic and Applied Sciences*, vol. 27, no. 1, pp. 149–165, 2020.

[13] L. J. Crane, "Flow past a stretching plate," *Zeitschrift für Angewandte Mathematik und Physik*, vol. 21, no. 4, pp. 645–647, 1970.

[14] P. Besthapu, R. U. Haq, S. Bandari, and Q. M. Al-Mdallal, "Mixed convection flow of thermally stratified MHD nanofluid over an exponentially stretching surface with viscous dissipation effect," *Journal of the Taiwan Institute of Chemical Engineers*, vol. 71, pp. 307–314, 2017.

[15] S. P. A. Devi and R. Kandasamy, "Effects of chemical reaction, heat and mass transfer on non-linear MHD flow over an accelerating surface with heat source and thermal stratification in the presence of suction or injection," *Communications in Numerical Methods in Engineering*, vol. 19, no. 7, pp. 513–520, 2003.

[16] T. Hayat, S. A. Shehzad, H. H. Al-Sulami, and S. Asghar, "Influence of thermal stratification on the radiative flow of Maxwell fluid," *Journal of the Brazilian Society of Mechanical Sciences and Engineering*, vol. 35, no. 4, pp. 381–389, 2013.

[17] T. Hayat, M. Waqas, S. A. Shehzad, and A. Alsaedi, "On 2D stratified flow of an Oldroyd-B fluid with chemical reaction: an application of non-Fourier heat flux theory," *Journal of Molecular Liquids*, vol. 223, pp. 566–571, 2016.

[18] M. Noor, S. Nadeem, and T. Mustafa, "Squeezed flow of a nanofluid with Cattaneo-Christov heat and mass fluxes," *Results in Physics*, vol. 7, pp. 862–869, 2017.

[19] Hashim and M. Khan, "On Cattaneo-Christov heat flux model for Carreau fluid flow over a slendering sheet," *Results in Physics*, vol. 7, pp. 310–319, 2017.

[20] J. Wasim, K. S. Nisar, R. W. Ibrahim, V. Tayyaba Mukhtar, and F. A. Vijayakumar, "Computational frame work of Cattaneo-Christov heat flux effects on engine oil based Williamson hybrid nanofluids: a thermal case study," *Case Studies in Thermal Engineering*, vol. 26, article 101179, 2021.

[21] B. C. Sakiadis, "Boundary-layer behavior on continuous solid surfaces: II. The boundary layer on a continuous flat surface," *AIChE Journal*, vol. 7, no. 2, pp. 221–225, 1961.

[22] B. O. Falodun, C. Onwubuoya, and F. H. Awoniran Alamu, "Magnetohydrodynamics (MHD) heat and mass transfer of Casson fluid flow past a semi-infinite vertical plate with thermophoresis effect: spectral relaxation analysis," *Defect and Diffusion Forum*, vol. 389, pp. 18–35, 2018.

[23] A. S. Idowu and B. O. Falodun, "Soret-Dufour effects on MHD heat and mass transfer of Walter's-B viscoelastic fluid over a semi-infinite vertical plate: spectral relaxation analysis," *Journal of Taibah University*, vol. 13, no. 1, pp. 49–62, 2019.

[24] A. S. Idowu and B. O. Falodun, "Variable thermal conductivity and viscosity effects on non-Newtonian fluids flow through a vertical porous plate under Soret-Dufour influence," *Mathematics and Computers in Simulation*, vol. 177, pp. 358–384, 2020.

[25] F. D. Ayegbusi, C. Onwubuoya, and B. O. Falodun, "Unsteady problem of magnetohydrodynamic heat plus mass transfer convective flow over a moveable plate with effects of thermophoresis and thermal radiation," *Heat Transfer*, vol. 49, no. 6, pp. 3593–3612, 2020.

[26] L. O. Ahmed, B. O. Falodun, and J. Abdulwaheed, "Mechanism of Soret-Dufour, magnetohydrodynamics, heat and mass transfer flow with buoyancy force, and viscous dissipation effects," *Heat Transfer*, vol. 49, no. 5, pp. 2831–2848, 2021.

[27] B. O. Falodun and F. D. Ayegbusi, "Soret–Dufour mechanism on an electrically conducting nanofluid flow past a semi-infinite porous plate with buoyancy force and chemical reaction influence," *Numerical Methods for Partial Differential Equations*, vol. 37, no. 2, pp. 1419–1438, 2021.

[28] M. M. Bhatti and S. I. Abdelsalam, "Bio-inspired peristaltic propulsion of hybrid nanofluid flow with tantalum (Ta) and gold (Au) nanoparticles under magnetic effects," in *Waves in Random and Complex Media*, pp. 1–26, Taylor & Francis, 2021.

[29] R. E. Abo-Elkhair, M. M. Bhatti, and K. S. Mekheimer, "Magnetic force effects on peristaltic transport of hybrid bio-nanofluid (Au Cu nanoparticles) with moderate Reynolds number: an expanding horizon," *International Communications in Heat and Mass Transfer*, vol. 123, article 105228, 2021.

[30] A. S. Idowu and B. O. Falodun, "Influence of magnetic field and thermal radiation on steady free convective flow in a porous medium," *Nigerian Journal of Technological Development*, vol. 15, no. 3, pp. 84–97, 2018.

[31] L. Zhang, M. M. Bhatti, E. E. Michaelides, E. Efstathios, M. Marin, and R. Ellahi, "Hybrid nanofluid flow towards an elastic surface with tantalum and nickel nanoparticles under the influence of an induced magnetic field," *The European Physical Journal Special Topics*, vol. 231, no. 3, pp. 521–533, 2022.

[32] U. Himanshu, A. K. Pandey, and M. Kumar, "Assessment of entropy generation and heat transfer in three-dimensional hybrid nanofluids flow due to convective surface and base fluids," *Journal of Porous Media*, vol. 24, no. 3, pp. 35–50, 2021.

[33] J. Narneet, A. K. Pandey, H. Upreti, and M. Kumar, "Mixed convection flow of magnetic hybrid nanofluid over a bidirectional porous surface with internal heat generation and a higher-order chemical reaction," *Heat Transfer*, vol. 50, no. 4, pp. 3661–3682, 2021.

[34] A. S. Idowu, M. T. Akolade, J. U. Abubakar, and B. O. Falodun, "MHD free convective heat and mass transfer flow of dissipative Casson fluid with variable viscosity and thermal conductivity effects," *Journal of Taibah University for Science*, vol. 14, no. 1, pp. 851–862, 2020.

[35] B. O. Falodun, A. A. Ayoade, and O. Odetunde, "Positive and negative Soret and Dufour mechanism on unsteady heat and mass transfer flow in the presence of viscous dissipation, thermal and mass buoyancy," in *Australian Journal of Mechanical Engineering*, pp. 1–14, Taylor & Francis, 2021.

[36] U. Himanshu, P. A. Kumar, R. S. Kumar, and K. Manoj, "Modified Arrhenius and thermal radiation effects on three-dimensional magnetohydrodynamic flow of carbon nanotubes nanofluids over bi-directional stretchable surface," *Journal of Nanofluids*, vol. 10, no. 4, pp. 538–551, 2021.

[37] K. Singh, A. K. Pandey, and M. Kumar, "Numerical approach for chemical reaction and suction/injection impacts on magnetic micropolar fluid flow through porous wedge with Hall and ion-slip using Keller box method," in *Waves in Random and Complex Media*, pp. 1–26, Taylor & Francis, 2021.

[38] U. Himanshu, A. K. Pandey, and M. Kumar, "Thermophoresis and suction/injection roles on free convective MHD flow of Ag-kerosene oil nanofluid," *Journal of Computational Design and Engineering*, vol. 7, no. 3, pp. 386–396, 2020.

[39] G. V. Ramana Reddy, R. N. Bhaskar, and A. J. Chamkha, "MHD mixed convection oscillatory flow over a vertical surface in a porous medium with chemical reaction and thermal radiation," *Journal of Applied Fluid Mechanics*, vol. 9, no. 3, pp. 1221–1229, 2016.

[40] G. V. Ramana Reddy, R. N. Bhaskar, and R. S. R. Gorla, "Radiation and chemical reaction effects on MHD flow along a moving vertical porous plate," *International Journal of Applied Mechanics and Engineering*, vol. 21, no. 1, pp. 157–168, 2016.

[41] G. V. R. Reddy and Y. H. Krishna, "Numerical solutions of unsteady MHD flow heat transfer over a stretching surface with suction or injection," *Fluid Dynamics and Materials Processing*, vol. 14, no. 3, pp. 213–222, 2018.

[42] S. S. Motsa, "New iterative methods for solving nonlinear boundary value problems," in *Fifth Annual Workshop on Computational Applied Mathematics and Mathematical Modeling in Fluid Flow*, pp. 9–13, School of Mathematics, Statistics and Computer Science, Pietermaritzburg Campus, 2012.

[43] S. S. Motsa, P. G. Dlamini, and M. Khumalo, "Spectral relaxation method and spectral quasilinearization method for solving unsteady boundary layer flow problems," *Advances in Mathematical Physics*, vol. 2014, Article ID 341964, 12 pages, 2014.

[44] F. I. Alao, A. I. Fagbade, and B. O. Falodun, "Effects of thermal radiation, Soret and Dufour on an unsteady heat and mass transfer flow of a chemically reacting fluid past a semi-infinite vertical plate with viscous dissipation," *Journal of the Nigerian Mathematical Society*, vol. 35, no. 1, pp. 142–158, 2016.

[45] A. S. Idowu and B. O. Falodun, "Soret–Dufour effects on MHD heat and mass transfer of Walter's-B viscoelastic fluid over a semi-infinite vertical plate: spectral relaxation analysis," *Journal of Taibah University for Science*, vol. 13, no. 1, pp. 49–62, 2019.